

Tightly bound gap solitons in a Fermi gas

SADHAN K. ADHIKARI¹ and BORIS A. MALOMED²

¹ *Instituto de Física Teórica, UNESP – São Paulo State University, 01.405-900 São Paulo, São Paulo, Brazil*

² *Department of Physical Electronics, School of Electrical Engineering, Faculty of Engineering, Tel Aviv University, Tel Aviv 69978, Israel*

PACS 03.75.Ss – Degenerate Fermi gases

PACS 03.75.Lm – Tunneling, Josephson effect, Bose-Einstein condensates in periodic potentials, solitons, vortices, and topological excitations

PACS 05.45.Yv – Solitons

Abstract. - Within the framework of the mean-field-hydrodynamic model of a degenerate Fermi gas (DFG), we study, by means of numerical methods and variational approximation (VA), the formation of fundamental gap solitons (FGSs) in a DFG (or in a BCS superfluid generated by weak interaction between spin-up and spin-down fermions), which is trapped in a periodic optical-lattice (OL) potential. An effectively one-dimensional (1D) configuration is considered, assuming strong transverse confinement; in parallel, a proper 1D model of the DFG (which amounts to the known quintic equation for the Tonks-Girardeau gas in the OL) is considered too. The FGSs found in the first two bandgaps of the OL-induced spectrum (unless they are very close to edges of the gaps) feature a (*tightly-bound*) shape, being essentially confined to a single cell of the OL. In the second bandgap, we also find antisymmetric tightly-bound *subfundamental solitons* (SFSs), with zero at the midpoint. The SFSs are also confined to a single cell of the OL, but, unlike the FGSs, they are unstable. The predicted solitons, consisting of $\sim 10^4 - 10^5$ atoms, can be created by available experimental techniques in the DFG of ⁶Li atoms.

Introduction: Matter-wave solitons were created as localized nonlinear excitations in Bose-Einstein condensates (BECs) of attractively interacting ⁷Li [1] and ⁸⁵Rb [2] atoms loaded in a cigar-shaped trap. In both cases, the interaction was switched from repulsion to attraction by applying magnetic field near the Feshbach resonance [3,4]. In the absence of axial confinement, the solitons can propagate freely in the axial direction. This was followed by the creation of *gap solitons*, GSs (formed by a few hundred atoms of ⁸⁷Rb) in a self-repulsive BEC loaded in a cigar-shaped trapped combined with an optical lattice (OL) [5], which was created as the interference pattern by counter-propagating laser beams (see also review [6]). Theoretical description of the dilute BEC relies upon the Gross-Pitaevskii equation (GPE), which provides for a remarkably accurate description of various matter-wave patterns, including solitons [7]. In particular, GSs exist at values of the chemical potential that fall in finite gaps of the band spectrum of the linear problem, induced by the periodic OL potential. In that case, the system possesses a *negative effective mass*, which allows the formation of solitons in balance with the repulsive nonlinearity [8].

The quest for solitons in degenerate Fermi gases (DFGs), which are also available to experiments [9], is a new challenge. Quasi-soliton excitations in DFGs formed by noninteracting fermions were analyzed in refs. [10]. Solitons were predicted in fermion-boson mixtures [11,12] which feature strong fermion-boson attraction. Currently, ⁶Li-⁷Li [13], ⁶Li-²³Na [14], and ⁴⁰K-⁸⁷Rb [15] mixtures of boson and fermion atoms are available, as well as binary DFGs, such as mixtures of two different spin states in ⁴⁰K [16] and ⁶Li [17] gases. Accordingly, solitons in a binary fermion gas with attraction between the two species have been predicted [18].

In this Letter, we aim at predicting solitons of the gap type in a DFG trapped in the OL, using a mean-field hydrodynamic (MFHD) model of the DFG, which actually stems from an approximation of the Thomas-Fermi type [19,20]. While the MFHD equations do not grasp effects of the multi-particle coherence, they provide a reasonably accurate description of various macroscopic patterns in DFGs, including the formation of solitons [21] and miscibility-immiscibility transition in binary gases [22]. As explained below, essentially the same equations may also

apply to a different setting, *viz.*, a BCS (Bardeen-Cooper-Schrieffer) superfluid formed in the gas of fermions due to a weak attraction between atoms with opposite polarizations of the spin; the attraction may be induced by means of the Feshbach-resonance technique too.

We consider three versions of the 1D MFHD equation for the fermion wave function. The most fundamental one is derived from the underlying 3D Fermi distribution, assuming a quasi-1D (cigar-shaped) trap with the radius of the transverse confinement, a_{\perp} , larger than the de Broglie wavelength, λ_F , of atoms on the Fermi surface. In this case, the MFHD equation for wave function ψ contains the self-repulsive nonlinear term $|\psi|^{4/3}\psi$. In the opposite case of an extremely tight transverse confinement, with $a_{\perp} \ll \lambda_F$, the underlying Fermi distribution is one-dimensional, leading to an equation with the repulsive quintic term, $|\psi|^4\psi$, the same as in the version of the GPE derived in ref. [23] for the Tonks-Girardeau gas. Solitons in the 1D equation combining the quintic term and the OL potential were recently considered in refs. [24]. One may also consider an anisotropic trap, with $a_{\perp} \gtrsim \lambda_F$ in one transverse direction and $a_{\perp} \ll \lambda_F$ in the other. Then, the underlying 2D Fermi distribution gives rise to an equation with the self-repulsive cubic term, $|\psi|^2\psi$, formally the same as in the ordinary BEC.

GS solutions to the GPE with the repulsive nonlinearity are usually assumed to be loosely bound ones, featuring weak localization and wavy tails, see, e.g., refs. [24]. We are interested in a possibility to predict GSs of a different kind, *tightly-bound* ones, localized practically in a single cell of the OL (cf. refs. [25], [26], and [27], where both loosely and tightly bound GSs were investigated in BEC models). We demonstrate that this is the case indeed, except when the chemical potential is very close to edges of the bandgap (in that case, GSs start to develop wavy tails, signaling a transition to delocalized states in the Bloch bands). We report families of symmetric (even) *fundamental gap solitons* (FGSs), originating in the first bandgap and continuing into the second gap, which feature a waveform with a single maximum, and antisymmetric (odd) *subfundamental gap solitons* (SFSs, the name borrowed from ref. [25]), that emerge in the second bandgap, with two maxima in the density profile and a zero between them, all squeezed into a single OL cell.

Below, we study these solitons by means of numerical simulations and variational approximation (VA) [28]. The VA, based on the Gaussian ansatz, predicts the FGS families, in terms of the dependence between the effective nonlinearity and chemical potential, in the first two bandgaps with a surprisingly high accuracy, if compared to numerical results. SFSs are predicted too, although less accurately, in the second bandgap, by means of another (antisymmetric) ansatz. We also report examples of stable symmetric and antisymmetric bound states of the FGSs.

The models We derive the MFHD equation for the fermion wave function, Ψ , as an extension of the static Thomas-Fermi distribution of the atomic density, $n =$

$|\Psi|^2$, which is [19, 20]

$$V(\mathbf{r}) + V_{\text{eff}}^{\mathcal{D}} = \mu, \quad (1)$$

with μ the chemical potential, $V(\mathbf{r})$ the external trapping potential, and $V_{\text{eff}}^{\mathcal{D}}$ an effective nonlinear potential in the \mathcal{D} -dimensional space accounting for the Fermi pressure. For $\mathcal{D} \equiv 3\text{D}$, 2D , and 1D , the role of $V_{\text{eff}}^{(\mathcal{D})}$ is actually played by the local Fermi energy, ε_F , expressed in terms of local atomic density $n_{\mathcal{D}}$, which is defined as per the dimension [20]. This yields $(2m/\hbar^2)V_{\text{eff}}^{(\mathcal{D})} = (6\pi^2 n_{3\text{D}})^{2/3}$, $4\pi n_{2\text{D}}$, and $(\pi n_{1\text{D}})^2$, respectively, with m the atom mass. The MFHD equation for stationary problems is derived by treating relation (1) as one which defines the effective Thomas-Fermi Hamiltonian in terms of $V_{\text{eff}}^{\mathcal{D}}$. Augmenting the Hamiltonian with the kinetic-energy term and applying it to the wave function, one arrives at the stationary equation [20],

$$-\frac{\hbar^2}{2m}\nabla_{\mathcal{D}}^2\Psi + [V(\mathbf{r}) + V_{\text{eff}}^{\mathcal{D}}]\Psi = \mu\Psi. \quad (2)$$

A dynamic version of eq. (2) is [20]

$$-\frac{\hbar^2}{2m}\nabla_{\mathcal{D}}^2\psi + [V(\mathbf{r}) + V_{\text{eff}}^{\mathcal{D}}]\psi = i\hbar\frac{\partial\psi}{\partial t}, \quad (3)$$

with $\psi(\mathbf{r}, t) = e^{-i\mu t/\hbar}\Psi(\mathbf{r})$, although this generalization is formal, as the above-mentioned derivation does not define the phase of the fermion wave function. Nevertheless, the dynamical equation, if it is treated as a phenomenologically postulated one, may yield reasonable predictions for stability of static MFHD states in the DFG [12, 18, 20].

As mentioned above, dynamical equation (3) can also be derived in a different physical context, for a BCS superfluid formed by Cooper pairs of fermions with opposite polarizations of the spin. Indeed, using the known expression for the local energy density of the superfluid in 3D [29], $\mathcal{E}_{3\text{D}} = (3/5)n_{3\text{D}}\varepsilon_F$ (recall ε_F is the local Fermi energy), and deriving the equation for the wave function of the Cooper pairs (alias the complex order parameter, in terms of the Ginzburg-Landau approach) from the Lagrangian density which includes term $\mathcal{E}_{3\text{D}}$, one will end up with a 3D equation that differs from the 3D version of eq. (3) only by a numerical factor in front of $V_{\text{eff}}^{\mathcal{D}}$. In a similar fashion, using the local density of the BCS superfluid in 1D [30] and 2D settings, $\mathcal{E}_{1\text{D}} = (1/3)n_{3\text{D}}\varepsilon_F$ and $\mathcal{E}_{2\text{D}} = (1/2)n_{2\text{D}}\varepsilon_F$, one can derive the respective 1D and 2D equations, which differ from their counterparts (7) and (6) written below only by numerical coefficients in front of the nonlinear terms.

In the case of the ordinary cigar-shaped waveguide with strong harmonic confinement in the transverse plane, eq. (3) and its static version, eq. (2), can be reduced to the 1D form by means of the well-known substitution [31], $\psi(x, y, z, t) = \phi(x, t) \exp[-i\omega_{\perp}t - (y^2 + z^2)/(2a_{\perp}^2)]$, with the second multiplier representing the ground state of the transverse

harmonic oscillator, ω_\perp is the respective frequency, and $a_\perp = \sqrt{\hbar/(m\omega_\perp)}$. The substitution of this ansatz in eq. (3) for $\mathcal{D} = 3\text{D}$ and averaging in the transverse plane yield the effective 1D equation,

$$i\hbar\phi_t = -\frac{\hbar^2}{2m}\phi_{xx} + \frac{3\hbar^2}{10m} \left[6\pi^2 |\phi|^2 \right]^{2/3} \phi - \epsilon \cos\left(\frac{4\pi}{\lambda}x\right) \phi, \quad (4)$$

where the OL potential with strength ϵ and period $\lambda/2$ is introduced. Equation (4) is further rescaled by defining $\phi \equiv \sqrt{2N/\lambda a_\perp^{-1}} \tilde{\phi}$, $t \equiv \lambda^2 m / (4\pi^2 \hbar) \tilde{t}$, $x \equiv \lambda \tilde{x} / (2\pi)$, $V_0 = \epsilon m \lambda^2 / (2\pi \hbar)^2$, where N is the number of atoms. The result is

$$i\phi_t = -(1/2)\phi_{xx} + g_{3\text{D}} |\phi|^{4/3} \phi - V_0 \cos(2x) \phi \quad (5)$$

(tildes are dropped here), with the wave function subject to normalization $\mathcal{N} \equiv \int_{-\infty}^{+\infty} |\phi(x)|^2 dx = 1$, and effective strength of the nonlinearity and potential defined as $g_{3\text{D}} = (3/10) [3N\lambda^2 / (2\pi a_\perp^2)]^{2/3}$ (subscript 3D refers to the derivation of the equation from the 3D Fermi distribution), $V_0 = m\epsilon (\lambda/2\pi\hbar)^2$. Similarly, the following normalized 1D equations can be derived from the underlying 2D and 1D Fermi distributions:

$$i\phi_t = -\frac{1}{2}\phi_{xx} + g_{2\text{D}} |\phi|^2 \phi - V_0 \cos(2x) \phi, \quad (6)$$

$$i\phi_t = -\frac{1}{2}\phi_{xx} + g_{1\text{D}} |\phi|^4 \phi - V_0 \cos(2x) \phi, \quad (7)$$

with $g_{2\text{D}} = \lambda N / (\sqrt{\pi} a_\perp)$, $g_{1\text{D}} = \pi^2 N^2 / 2$.

Stationary solutions to eqs. (5), (6), and (7) are looked for in the usual form, $\phi(x, t) = e^{-i\mu t} u(x)$, with real function u obeying the equation

$$\mu u + (1/2)u'' - g u^{\aleph_{\mathcal{D}}} + V_0 \cos(2x) u = 0, \quad (8)$$

where $\aleph_{\mathcal{D}} = 7/3, 3, 5$, respectively, for $\mathcal{D} = 3\text{D}, 2\text{D}, 1\text{D}$. In fact, the static 1D equations (8) for the real wave function have the straightforward physical meaning, within the framework of the MFHD description, while their dynamic counterparts for the complex wave function are more formal ones, as mentioned above. Nevertheless, the dynamical equations are quite useful, as their direct simulations converge to real stationary states that represent numerically exact solutions to the static equations (see below). Besides that, the dynamical equations make sense (similar to the time-dependent Ginzburg-Landau equations) if applied, as mentioned above, to the BCS superfluid. Our main objective is to find a family of FGS solutions to eq. (8) with μ falling in the first two finite bandgaps of the linear spectrum.

Variational approximation Equation (8) and the above normalization condition, $\mathcal{N} = 1$, can be derived as the variational equations [28], $\delta L / \delta u = \partial L / \partial \mu = 0$, from the Lagrangian,

$$L = \int_{-\infty}^{+\infty} \left[\mu u^2 - \frac{1}{2} (u')^2 - \frac{2g}{\aleph_{\mathcal{D}} + 1} u^{\aleph_{\mathcal{D}} + 1} + V_0 \cos(2x) \cdot u^2 \right] dx - \mu. \quad (9)$$

To apply the VA, we use a simple Gaussian ansatz [28],

$$u(x) = \pi^{-1/4} \sqrt{\mathcal{N}/W} \exp[-x^2 / (2W^2)], \quad (10)$$

where variational parameters are the soliton's norm and width, \mathcal{N} and W (in addition to μ). The substitution of this ansatz in Lagrangian (9) yields

$$L = \mu(\mathcal{N} - 1) - \frac{\mathcal{N}}{4W^2} + V_0 \mathcal{N} N e^{-W^2} - \frac{2^{3/2} g}{\pi^{\aleph_{\mathcal{D}}/2} (\aleph_{\mathcal{D}} + 1)^{3/2}} \frac{\mathcal{N}^{(\aleph_{\mathcal{D}} + 1)/2}}{W^{(\aleph_{\mathcal{D}} - 1)/2}}. \quad (11)$$

The corresponding variational equations, $\partial L / \partial \mu = \partial L / \partial W = \partial L / \partial \mathcal{N} = 0$, lead to $\mathcal{N} = 1$ (as expected), and

$$1 + \frac{2^{3/2} (\aleph_{\mathcal{D}} - 1) g}{\pi^{(\aleph_{\mathcal{D}} - 1)/4} (\aleph_{\mathcal{D}} + 1)^{3/2}} W^{(5 - \aleph_{\mathcal{D}})/2} = 4V_0 W^4 e^{-W^2}, \quad (12)$$

$$\mu = \frac{1}{4W^2} + \frac{\sqrt{2}g}{(\pi W^2)^{(\aleph_{\mathcal{D}} - 1)/4} \sqrt{\aleph_{\mathcal{D}} + 1}} - V_0 e^{-W^2}. \quad (13)$$

Then, eqs. (12) and (13) were solved numerically.

Results Simulations of eqs. (5), (6), and (7) were carried out by dint of a real-time integration method based on the Crank-Nicholson discretization scheme, as elaborated in ref. [32]. The equations were discretized using time and space steps 0.0005 and 0.025, respectively, in domain $-20 < x < 20$. To find FGSs, the simulations started with an initial configuration chosen as the ground state, $\phi(x) = (\sqrt{2}c/\pi)^{1/4} \exp[-x^2 \sqrt{c/2}]$, of the linear oscillator with potential cx^2 (with $c \gg 1$, typically 5 to 100). The OL potential was slowly introduced in the course of the simulations. The strong harmonic potential squeezes the localized state into a single cell of the OL. After obtaining a stationary bound state in the nonlinear equation containing the combined OL and harmonic potential, the latter one was slowly switched off. The simulations were run until a well-defined stationary shape of the soliton was established. A similar approach to the creation of GSs in BEC was proposed in ref. [33]. To generate SFS solutions (see below), the initial state was taken as the first excited state of the above-mentioned harmonic potential, instead of its ground state. We present results for a characteristic value of the OL strength, $V_0 = 5$.

Families of FGS solutions are characterized by the corresponding dependences, $g_{\mathcal{D}}(\mu)$. In fig. 1, they are displayed as found from the numerical solution of the 1D, 2D, and 3D models, along with the same dependences as predicted, for the three models, by the VA.

In fig. 2 we display typical profiles of the solitons. It is obvious that the FGSs, unless taken too close to bandgap edges, are compact objects, primarily trapped in a single cell of the OL. There also exist more loosely organized localized states, which occupy several cells [24], that we do not consider here. Figure 2 demonstrates that the VA produces a very good fit not only to the $g(\mu)$ plots for the

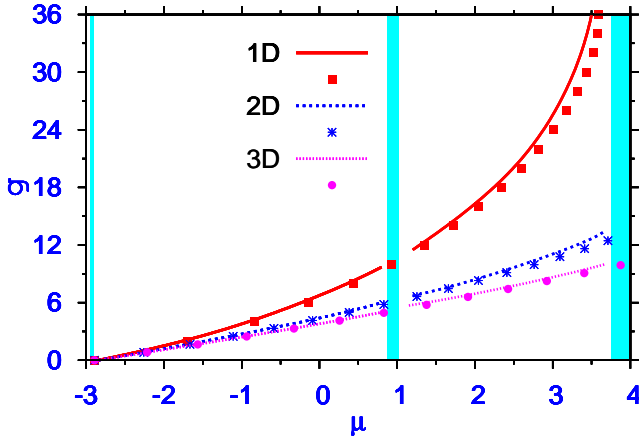


Fig. 1: Numerical (continuous curve) and variational (chain of symbols) results for nonlinearity g versus chemical potential μ , for fundamental gap solitons in the first and second finite bandgaps of periodic potential $-V_0 \cos(2x)$, (all results reported in this Letter with $V_0 = 5$), in the models based on eqs. (7), (6), and (5) (“1D”, “2D”, and “3D”, respectively, which refers to the dimension of the underlying Fermi distribution, from which the equation is derived). The shaded areas represent the Bloch bands.

entire soliton families (see fig. 1), but also to FGS profiles in the two lowest finite gaps, except very close to edges of the gaps, where the solitons develop undulate tails, that simple ansatz (10) is unable to reproduce [see panels in fig. 2 pertaining to $g = 0.01$]. In principle, GSs with conspicuous tails may be approximated by a more complex ansatz, which combines the Gaussian and function $\cos x$; however, variational equations generated by such an ansatz are very cumbersome, and, in the end, the extended ansatz does not approximate the entire tail, but only its secondary peaks which are closest to the central one [27]. For this reason, we do not try to apply that ansatz here.

It is relevant to mention that as the chemical potential moves closer to the Bloch band the wave form of the GSs develop a structure in space similar to Wannier functions, which are spatially localized linear combinations of Bloch functions. Figure 2 (a) shows the wave form near the edges of the gap. The undulate tails in this figure signal the proximity to a Bloch band, where the wave form will turn into a periodic structure. However, as said above, such wave forms cannot be fitted to Gaussian shapes and we do not intend to study them in detail here.

Within the framework of eqs. (5) - (7), the stability of the FGSs was tested by subjecting them to relatively strong initial perturbations (as said above, the dynamical equations have direct meaning in the application to the BCS superfluid). It has been found that the entire families of these solutions are stable, in all the three above-mentioned models, see a typical example in Fig. 3. In the case displayed in this figure, after the stationary FGS

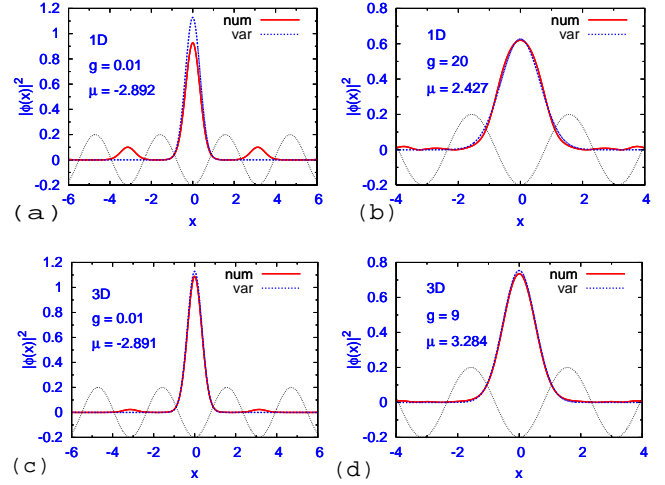


Fig. 2: Typical shapes of the fundamental gap solitons in the model derived from the 1D Fermi distribution, Eq. (7), for (a) $g_{1D} = 0.01$, ($\mu = -2.892$), (b) $g_{1D} = 20$ ($\mu = 2.427$), and from the 3D distribution, Eq. (5), for (c) $g_{3D} = 0.01$, ($\mu = -2.891$), and (d) $g_{3D} = 9$, ($\mu = 3.284$). Shapes produced by the numerical solution and variational approximation are labeled as “num” and “var”. The panels pertaining to $g_{3D} = g_{1D} = 0.01$ display the solitons very close to the left edge of the first bandgap, while the panels for $g_{1D} = 20$ and $g_{3D} = 9$ give typical examples found inside the second bandgap (inside the first gap, the shape of the fundamental solitons is quite similar). The thin sinusoidal line (in this and following figures) depicts the profile of the underlying OL potential.

of the model based on the 3D Fermi distribution was obtained (for $g_{3D} = 9$), we replaced, at $t = 20$, the stationary wave form $\phi(x)$ by a perturbed one, $1.2\phi(x)$, and continued the simulation. The resultant solution demonstrates persistent oscillations, and no sign of degradation.

The usual GPE, with the repulsive cubic nonlinearity and OL potential, i.e., eq. (6), gives rise to antisymmetric SFSs, the family of which starts at the left edge of the second finite bandgap [25]. A characteristic feature of the SFSs is that two maxima of the density, $|\phi(x)|^2$, are located inside a single site of the periodic potential (i.e., this antisymmetric soliton as a whole is confined to a single site). To look for SFSs in the present models, we applied the VA based on the modified Gaussian ansatz (cf. eq. (10)),

$$u(x) = \pi^{-1/4} \left(\sqrt{2N}/W^{3/2} \right) x \exp(-x^2/(2W^2)), \quad (14)$$

where N and W have the same meaning as in eq. (10). The substitution of ansatz (14) in Lagrangian (9) yields

$$L = \mu(\mathcal{N} - 1) - \frac{3\mathcal{N}^2}{4W^2} + V_0 \mathcal{N} e^{-W^2} (1 - 2W^2) - \frac{2^{\mathcal{N}_D+5/2} g \Gamma(1 + \mathcal{N}_D/2)}{\pi^{(\mathcal{N}_D+1)/4} (\mathcal{N}_D + 1)^{(\mathcal{N}_D+4)/2}} \frac{\mathcal{N}^{(\mathcal{N}_D+1)/2}}{W^{(\mathcal{N}_D-1)/2}}, \quad (15)$$

and the variational equations following from here are $\mathcal{N} =$

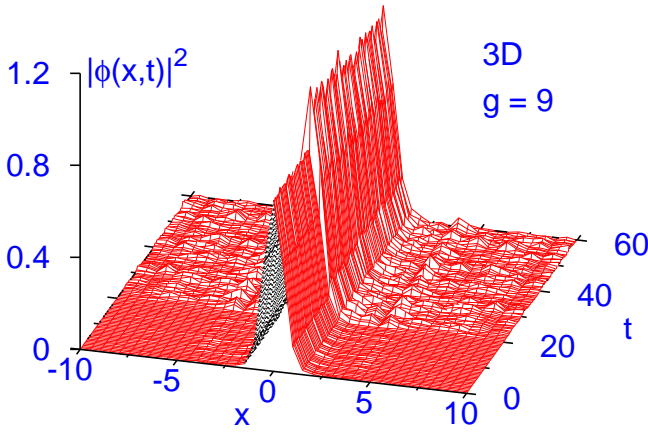


Fig. 3: An example of stable evolution of a fundamental gap soliton solution in the 3D model [eq. (5)], for $g_{3D} = 9$ of Fig. 2 (d). To introduce a perturbation, at $t = 20$, the wave form was suddenly multiplying by 1.2: $\phi(x, t) \rightarrow 1.2 \times \phi(x, t)$. The so perturbed soliton (as well as ones subjected to different arbitrary perturbations) remained stable as long as the simulations were run.

1 and

$$1 + \frac{\aleph_{\mathcal{D}} - 1}{3} \frac{2^{(2\aleph_{\mathcal{D}}+5)/2} g W^{(5-\aleph_{\mathcal{D}})/2}}{\pi^{(\aleph_{\mathcal{D}}+1)/4} (\aleph_{\mathcal{D}} + 1)^{(4+\aleph_{\mathcal{D}})/2}} \Gamma(\aleph_{\mathcal{D}}/2 + 1) = (4/3) V_0 W^4 e^{-W^2} (3 - 2W^2), \quad (16)$$

$$\mu = \frac{3}{4W^2} + \frac{2^{(2\aleph_{\mathcal{D}}+3)/2} g}{\pi^{(\aleph_{\mathcal{D}}+1)/4} (\aleph_{\mathcal{D}} + 1)^{(2+\aleph_{\mathcal{D}})/2}} \frac{\Gamma(\aleph_{\mathcal{D}}/2 + 1)}{W^{\aleph_{\mathcal{D}}-1/2}} - V_0 e^{-W^2} (1 - 2W^2). \quad (17)$$

Numerical solution of eqs. (16) and (17) gives rise to SFS families in the second bandgap. The comparison of the corresponding characteristics $g(\mu)$ with their numerically found counterparts is presented in fig. 4(a). The accuracy of the VA predictions for the SFS families is worse than for the FGS solutions; nevertheless, the prediction is qualitatively correct.

Although the SFS families were found from direct simulations of eqs. (5), (6), and (7), hence they are, at least, quasi-stable solutions, longer simulations reveal their instability (not shown here). Similar to what was found in ref. [25] in the GPE with the cubic nonlinearity, which coincides with eq. (6), in all the three models considered here, the instability tends to transform the SFS (double-humped) solitons into a stable FGS (single-humped).

In addition to the SFSs, symmetric and antisymmetric (“twisted”, in the latter case) bound states of FGSs were found too. Typical examples of such stable bound states in the 3D and 1D models are shown in figs. 5(a) and (b), respectively. The antisymmetric state is formally similar to the SFS, but a difference is that the density maxima of the bound state are located in different OL sites. Direct simulations (not shown here) clearly demonstrate that both

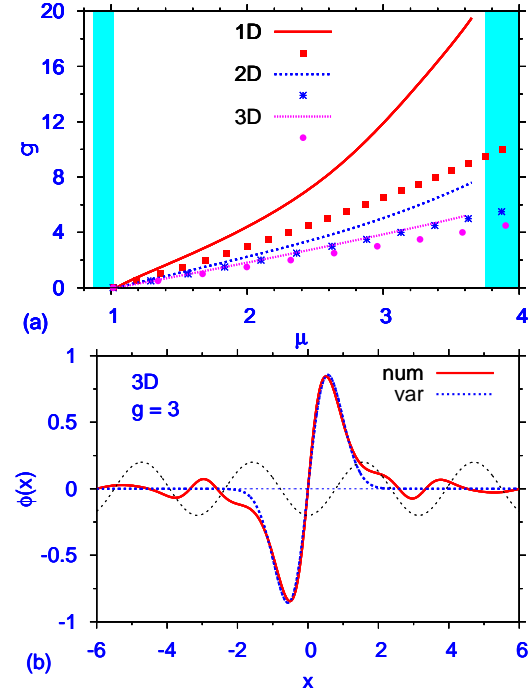


Fig. 4: (a) The same as in fig. 1, but for families of subfundamental gap solitons. (b) A typical example of the subfundamental soliton, obtained from the numerical solution of eq. (5) (for $g_{3D} = 3$), and its counterpart predicted by the VA.

symmetric and antisymmetric bound states are stable one (on the contrary to the SFS solutions).

Conclusion In the three MFHD models, based on eqs. (7), (6), and (5), we have considered, by means of numerical simulations and VA (variational approximation), the generation of stable fundamental and unstable subfundamental gap solitons (FGSs and SFSs, respectively) in the quasi-1D degenerate Fermi gas loaded in a periodic OL potential. The same models apply to the BCS superfluid trapped in the OL. In most cases, both the FGSs and SFSs are confined, essentially, to a single cell of the lattice. The VA provides a very good fit to the FGSs, and a qualitatively correct approximation for the SFSs. Stable symmetric and antisymmetric bound states of the FGSs were also found. It was demonstrated that transport of the FGSs, without much distortion, is possible by a slowly moving OL.

Experimental realization of the FGSs in degenerate Fermi gases seems quite feasible. To this end, the gas should be loaded in a cigar-shaped trap combined with the periodic axial potential, as was done to create gap solitons in the BEC [5,6]. The experiment may be started with an additional strong parabolic potential acting in the axial direction, to prepare a strongly localized state, that may have a good chance to self-trap into a tightly bound soliton while the extra potential is gradually switched off. An estimate for the ${}^6\text{Li}$ gas, with typical values of physical parameters, predicts that the FGSs based on the 3D

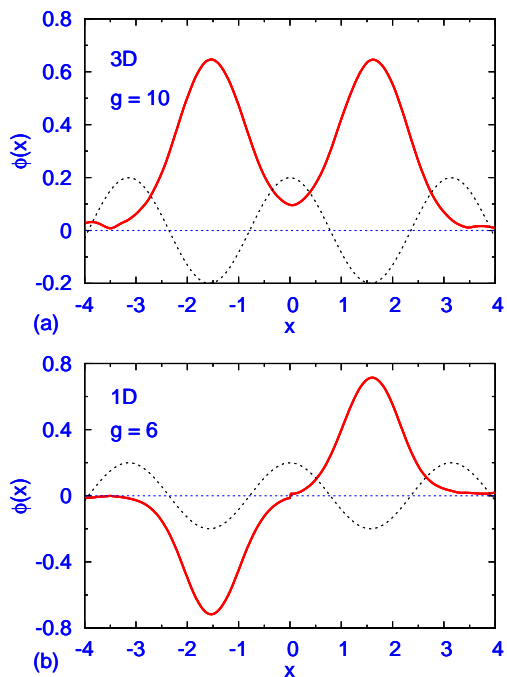


Fig. 5: Examples of stable symmetric (a) and antisymmetric (b) bound states of fundamental gap solitons in the models based on the 3D [Eq. (5)] and the 1D [Eq. (7)] Fermi distributions, respectively, for (a) $g_{3D} = 10$ and (b) $g_{1D} = 6$.

Fermi distribution, i.e., obeying eq. (5), may be created with $10^4 - 10^5$ atoms per soliton.

The work of B.A.M. was supported, in a part, by Israel Science Foundation through the grant No. 8006/03. The work of S.K.A. was supported, in a part, by FAPESP and CNPq of Brazil.

REFERENCES

- [1] Pérez-García V. M. *et al.*, *Phys. Rev. A*, **57** (1998) 3837; Strecker K. E. *et al.*, *Nature*, **417** (2002) 150; Khaykovich L. *et al.*, *Science*, **256** (2002) 1290; Cornish S. L. *et al.*, *Phys. Rev. Lett.*, **96** (2006) 170401.
- [2] Cornish S. L., Thompson S. T., and Wieman C. E., *Phys. Rev. Lett.* **96** (2006) 170401.
- [3] Inouye S. *et al.*, *Nature*, **392** (1998) 151.
- [4] Zaccanti M. *et al.*, *Phys. Rev. A*, **74** (2006) 041605(R); Ospelkaus S. *et al.*, *Phys. Rev. Lett.*, **97** (2006) 120403.
- [5] Eiermann B. *et al.*, *Phys. Rev. Lett.*, **92** (2004) 230401.
- [6] Morsch O. and Oberthaler M., *Rev. Mod. Phys.*, **78** (2006) 179.
- [7] Strecker K. E. *et al.*, *New J. Phys.*, **5** (2003) 73; Brazhnyi V. A. and Konotop V. V., *Mod. Phys. Lett. B*, **18** (2004) 627; Abdullaev F. Kh. *et al.*, *Int. J. Mod. Phys. B*, **19** (2005) 3415.
- [8] Alfimov G. L. *et al.*, *Europhys. Lett.*, **58** (2002) 7; Baizakov B. B. *et al.*, *J. Phys. B* **35** (2002) 51015; Louis P. J. Y. *et al.*, *Phys. Rev. A* **67** (2003) 013602.
- [9] DeMarco B. and Jin D. S., *Science*, **285** (1999) 1703; Minguzzi A. *et al.*, *Phys. Rep.*, **395** (2004) 223; Chen Q. J. *et al.*, *Phys. Rep.*, **412** (2005) 1.
- [10] Karpiuk T. *et al.*, *Phys. Rev. A*, **66** (2002) 023612; Witkowska E. and Brewczyk M., *Phys. Rev. A*, **72** (2005) 023606.
- [11] Karpiuk T. *et al.*, *Phys. Rev. Lett.*, **93** (2004) 100401; T. Karpiuk T. *et al.*, *Phys. Rev. A*, **73** (2006) 053602.
- [12] Adhikari S. K., *Phys. Rev. A*, **72** (2005) 053608; Salasnich L. *et al.*, *Phys. Rev. A*, **75** (2007) 023616; Adhikari S. K., *J. Phys. A*, **40** (2007) 2673.
- [13] Schreck F. *et al.*, *Phys. Rev. Lett.*, **87** (2001) 080403 (2001); Truscott A. G. *et al.*, *Science*, **291** (2001) 2570.
- [14] Hadzibabic Z. *et al.*, *Phys. Rev. Lett.*, **88** (2002) 160401.
- [15] Modugno G. *et al.*, *Science*, **297** (2002) 2240; Roati G. *et al.*, *Phys. Rev. Lett.*, **89** (2002) 150403.
- [16] DeMarco B. and Jin D. S., *Science*, **285** (1999) 1703.
- [17] O'Hara K. M. *et al.*, *Science*, **298** (2002) 2179; Strecker K. E. *et al.*, *Phys. Rev. Lett.*, **91** (2003) 080406.
- [18] Adhikari S. K., *Eur. Phys. J. D*, **40** (2006) 157; Adhikari S. K., *J. Phys. A*, **40** (2007) 2673.
- [19] Amoruso A. *et al.*, *Eur. Phys. J. D*, **8** (2000) 361; Roth R. and Feldmeier H., *J. Phys. B*, **34** (2001) 4629; Molmer K., *Phys. Rev. Lett.*, **80** (2004) 1804; Modugno M. *et al.*, *Phys. Rev. A*, **68** (2003) 043626; Jezek D. M. *et al.*, *Phys. Rev. A*, **70** (2004) 043630.
- [20] Capuzzi P. *et al.*, *Phys. Rev. A*, **67** (2003) 053605; **68** (2003) 033605.
- [21] Adhikari S. K., *New J. Phys.*, **8** (2006) 258; Adhikari S. K., *Phys. Rev. A*, **70**(2004) 043617.
- [22] Adhikari S. K. and Malomed B. A., *Phys. Rev. A*, **74** (2006) 053620; Adhikari S. K. and Salasnich L., *Phys. Rev. A*, **75** (2007) 053603; Adhikari S. K., *Phys. Rev. A*, **73** (2006) 043619.
- [23] Kolomeisky E. B. *et al.*, *Phys. Rev. Lett.*, **85** (2000) 1147.
- [24] Abdullaev F. Kh. and Salerno M., *Phys. Rev. A* **72** (2005) 033617; Alfimov G. L. *et al.*, *Phys. Rev. A*, **56** (2007) 023624; Salerno M., *Phys. Rev. A*, **72** (2005) 063602.
- [25] Maytevarunyo T. and Malomed B. A., *Phys. Rev. A*, **74** (2006) 033616.
- [26] Sakaguchi H. and Malomed B. A., *J. Phys. B*, **37** (2004) 1443; 2225; Gubeskys A., Malomed B. A., and Merhasin I. M., *Phys. Rev. A*, **73** (2006) 023607.
- [27] Gubeskys A., Malomed B. A., and Merhasin I. M., *Stud. Appl. Math.* **115** (2005) 255.
- [28] Pérez-García V. M. *et al.*, *Phys. Rev. A*, **56** (1997) 1424; Malomed B. A., in *Progress in Optics*, vol. 43, p. 71 (ed. by E. Wolf: North-Holland, Amsterdam, 2002).
- [29] Huang K. and Yang C. N. *Phys. Rev.* **105** (1957) 767; Lee T. D. and Yang C. N. *Phys. Rev.* **105** (1957) 1119.
- [30] Manini N. and Salasnich L. *Phys. Rev. A* **71** (2005) 033625.
- [31] Salasnich L., Parola A., and Reatto L., *Phys. Rev. A*, **65** (2002) 043614; **66** (2002), 043603.
- [32] Adhikari S. K. and Muruganandam P., *J. Phys. B*, **35** (2002) 2831. ; Muruganandam P. and Adhikari S. K., *J. Phys. B*, **36** (2003) 2501.
- [33] Matuszewski M. *et al.*, *Phys. Rev. A* **73** (2006) 063621.